



**HAL**  
open science

# Sunlight-driven photoinitiating systems for photopolymerization and application in direct laser writing

Ji Feng, Tong Gao, Fabrice Morlet-Savary, Michael Schmitt, Celine Dietlin,  
Jing Zhang, Pu Xiao, Frédéric Dumur, Jacques Lalevée

► **To cite this version:**

Ji Feng, Tong Gao, Fabrice Morlet-Savary, Michael Schmitt, Celine Dietlin, et al.. Sunlight-driven photoinitiating systems for photopolymerization and application in direct laser writing. *Polymer Chemistry*, 2024, 15 (28), pp.2899-2912. 10.1039/d4py00558a . hal-04649844

**HAL Id: hal-04649844**

**<https://hal.science/hal-04649844v1>**

Submitted on 16 Jul 2024

**HAL** is a multi-disciplinary open access archive for the deposit and dissemination of scientific research documents, whether they are published or not. The documents may come from teaching and research institutions in France or abroad, or from public or private research centers.

L'archive ouverte pluridisciplinaire **HAL**, est destinée au dépôt et à la diffusion de documents scientifiques de niveau recherche, publiés ou non, émanant des établissements d'enseignement et de recherche français ou étrangers, des laboratoires publics ou privés.

1 **Sunlight-driven photoinitiating systems for photopolymerization and**  
2 **application in direct laser writing**

3  
4 **Ji Feng<sup>a,b</sup>, Tong Gao<sup>a,b</sup>, Fabrice Morlet-Savary<sup>a,b</sup>, Michael Schmitt<sup>a,b</sup>, Celine**  
5 **Dietlin<sup>a,b</sup>, Jing Zhang<sup>c</sup>, Pu Xiao<sup>d\*</sup>, Frédéric Dumur<sup>e\*</sup>, and Jacques Lalevée<sup>a,b\*</sup>**  
6

7 <sup>a</sup> Université de Haute-Alsace, CNRS, IS2M UMR7361, F-68100 Mulhouse, France.

8 <sup>b</sup> Université de Strasbourg, France.

9 <sup>c</sup> Future Industries Institute, University of South Australia, Mawson Lakes, SA 5095,  
10 Australia.

11 <sup>d</sup> State Key Laboratory of High-Performance Ceramics and Superfine Microstructure,  
12 Shanghai Institute of Ceramics, Chinese Academy of Sciences, Shanghai 200050, P.  
13 R. China.

14 <sup>e</sup> Aix Marseille Univ, CNRS, ICR, UMR 7273, F-13397 Marseille, France.

15  
16 E-mail address: jacques.lalevee@uha.fr (J. L.); frederic.dumur@univ-amu.fr (F.D.);

17 p.xiao@mail.sic.ac.cn (P.X.)  
18

19 **Abstract:** Currently, there are only few industrial and academic works focused on  
20 photopolymerization conducted under natural light. Addressing this issue, six new dyes  
21 were synthesized as photosensitizers and combined with additives (an amine and an  
22 iodonium salt) to create three-component photoinitiation systems. These systems can  
23 efficiently initiate both the free radical polymerization (FRP) of an acrylate monomer  
24 and the cationic polymerization (CP) of an epoxy monomer. Remarkably, the FRP  
25 process, facilitated by these systems under natural sunlight, required only a low catalyst  
26 loading (0.1 wt% relative to monomer), and the conversion obtained with dye-B1 as  
27 the photosensitizer can reach 90% within 5 minutes. This highlights the viability of  
28 natural sunlight as an efficient light source for polymerization processes. More  
29 interestingly, dye-B1 can effectively initiate metal-free CP of an epoxy monomer. The  
30 chemical mechanism underlying photopolymerization was comprehensively elucidated  
31 through a combination of theoretical calculations, photolysis experiments, fluorescence  
32 quenching experiments, cyclic voltammetry (CV), and electron spin resonance spin  
33 trapping (ESR-ST) experiments. Leveraging the exceptional photocatalytic

34 performance of dye-B1, the corresponding three-component photoinitiating system was  
35 applied to 3D printing experiments, achieving high-precision 3D patterns via direct  
36 laser writing (DLW).

37

38 **Keywords:** Sunlight-induced polymerization; Metal-free cationic photopolymerization;  
39 Free radical photopolymerization; 3D printing; Green chemistry.

40

## 41 **1. Introduction:**

42 In the field of polymer synthesis, researchers are actively searching mild reaction  
43 conditions for performing photopolymerization. Inspired by natural processes like  
44 photosynthesis, which efficiently converts solar energy into chemical energy <sup>1</sup>, early  
45 innovators like Ciamician proposed the use of photocatalysts to mediate chemical  
46 reactions with light as early as 1912 <sup>2</sup>. Since then, photochemistry has continued to  
47 evolve with photocatalytic polymerization emerging as a promising alternative to  
48 traditional thermal polymerization methods due to its lower synthetic costs and reduced  
49 environmental impact. This shift has sparked considerable interest, particularly because  
50 photopolymerization techniques leverage clean energy sources such as solar radiation  
51 and offer potential applications <sup>3-5</sup> including solar cell power generation <sup>6</sup> and  
52 wastewater treatment.<sup>7</sup> Various energy-efficient light sources can initiate catalytic free  
53 radical polymerizations or cationic polymerizations <sup>8,9</sup>, including metal photocatalysts  
54 (fac-Ir(ppy)<sub>3</sub>, Ru(bpy)<sub>3</sub>Cl<sub>2</sub>, ZnTPP) <sup>10</sup>, semiconductor nano-quantum dot photocatalysts  
55 <sup>11</sup> and organic photocatalysts <sup>12</sup>. Considering that the metal-free photocatalytic systems  
56 have the advantages of environmental friendliness, low cost, and prevention of metal  
57 pollution in polymer products <sup>13</sup>, it has attracted significant attention in the polymer and  
58 or composite materials field <sup>3</sup>. Despite these advancements, many metal-free  
59 photocatalytic polymerization processes still rely on UV and UV-visible light sources,  
60 which pose environmental and experimental safety risks <sup>14,15</sup>. The high energy  
61 consumption and high cost associated with UV light sources also contradict principles  
62 of sustainable chemistry. Thus, there is a pressing need to harness solar energy for  
63 photocatalysis and enable large-scale industrialization.

64 Sunlight, as an abundant and sustainable energy source, holds immense potential  
65 for driving photopolymerization reactions <sup>1,2,16-19</sup>. However, the limited availability of  
66 efficient photocatalysts and the challenges posed by UV light sources have hindered  
67 widespread industrial adoption. This has spurred intensified research into  
68 photopolymerization using sunlight, particularly considering the broad emission  
69 spectrum of sunlight compared to the narrow emission spectra of LEDs.<sup>20-22</sup>. The  
70 pursuit of environmentally friendly and efficient photocatalytic polymerization induced  
71 by sunlight presents challenges, notably in achieving stability and usability under  
72 natural light conditions <sup>23</sup>. Despite recent research efforts, stability issues persist, with  
73 most studies focusing on LED-based systems rather than sunlight-induced reactions.<sup>24-</sup>  
74 <sup>26</sup>. Based on these statements, photocatalysts with remarkable photostability and  
75 excellent storage stability under sunlight and under air are actively researched. It is of  
76 great significance to develop such photoinitiating systems applicable for sunlight  
77 irradiation.

78 To address these challenges, we designed and synthesized a series of six new dyes  
79 for FRP and CP experiments. Remarkably, these metal-free dyes alone exhibit a good  
80 stability under sunlight, becoming reactive only when combined with co-initiators to  
81 form three-component photoinitiating systems. The six dyes could effectively induce  
82 the FRP of acrylates under sunlight, achieving an excellent curing of the resins within  
83 5 minutes of exposure. Notably, dye-B1 also successfully induced the CP of epoxides  
84 upon exposure to LED@405 nm offering intriguing possibilities for sunlight-induced  
85 reactions. The functional group transformation occurring during the polymerization  
86 reaction process was monitored using Real-Time Fourier Transform Infrared  
87 Spectroscopy (RT-FTIR), and then the mechanism involved in the polymerization  
88 process was elucidated in detail through photolysis experiments, fluorescence  
89 quenching, and ESR-ST experiments. Finally, the accurate 3D patterns obtained via  
90 direct laser write (DLW) technology underscores the practical application of our  
91 findings. This study represents a significant advancement in photopolymerization,  
92 offering an unprecedented reactivity under sunlight, the potential for using low  
93 photoinitiator content, and to get high conversion rates, paving the way for practical

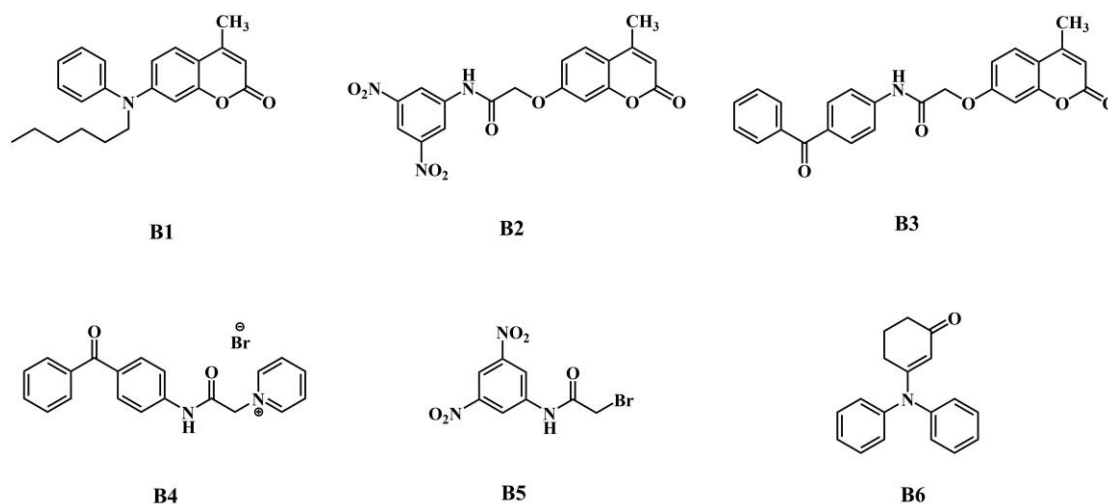
94 applications in various fields.

95

## 96 2. Experimental Process.

### 97 2.1 Dyes and other materials.

98 Six novel dyes were successfully synthesized and used for photopolymerization.  
99 The synthetic routes used to prepare these compounds are detailed in the following  
100 Section 3.1 and in supporting information. Chemical structures of the six dyes  
101 investigated in this work are shown in Figure 1. Other materials and structures of the  
102 monomers and co-initiators are shown in Figure S1 and supporting information.



103

104 **Figure 1.** Chemical structures of dyes B1-B6.

105

### 106 2.2 UV-vis absorption and fluorescence properties.

107 The UV-Vis absorption spectra and steady-state photolysis (dye-alone, dye/EDB,  
108 and dye/Iod) were recorded in acetonitrile under the irradiation of LED@405 nm  
109 (JASCO V730 spectrometer). The fluorescence spectra of dyes in acetonitrile and the  
110 quenching experiments of dyes by EDB or Iod were measured with a JASCO FP-6200  
111 fluorescence spectrometer. The electron transfer quantum yields ( $\phi_{et}$ ) were obtained by  
112 equation (1). The fluorescence excited state lifetime was measured with a HORIBA  
113 PPD-850 fluorometer.

$$114 \phi = \frac{K_{SV} * [\text{additive}]}{1 + K_{SV} * [\text{additive}]} \quad (1)$$

115 where the  $K_{SV}$  in the equation corresponds to the slope of Stern-Volmer treatment

116 in the fluorescence quenching experiment.

117

### 118 **2.3 Redox potentials of dyes obtained by cyclic voltammetry.**

119 Redox potentials (oxidation is  $E_{\text{ox}}$ , reduction is  $E_{\text{red}}$ ) of dyes were measured by CV.  
120 The different dyes and tetrabutylammonium hexafluorophosphate used as the support  
121 electrolyte were dissolved in acetonitrile and determined under nitrogen atmosphere.  
122 The singlet excited state energy level ( $E_{\text{S1}}$ ) of the dyes was determined from the  
123 intersection of the normalized UV-visible absorption and fluorescence spectra.  
124 Similarly, the triplet energy level ( $E_{\text{T1}}$ ) determined by molecular modeling (Gaussian  
125 03). According to the Rehm-Weller equation<sup>27,28</sup>, the change of free energy from the  
126 singlet excited state ( $\Delta G^{\text{S1}}_{\text{EDB}}$  or  $\Delta G^{\text{S1}}_{\text{Iod}}$ ) and the triplet free energy ( $\Delta G^{\text{T1}}_{\text{EDB}}$  or  $\Delta G^{\text{T1}}_{\text{Iod}}$ )  
127 in the electron transfer reaction between dyes and additives can be calculated. In  
128 particular, the  $E_{\text{ox}}$  of amine (EDB) is 1.0 V, and  $E_{\text{red}}$  of iodonium salt (Iod) is -0.7 V.

129

### 130 **2.4 FRP and metal-free CP under UV/visible-light irradiation and high-** 131 **performance sunlight-induced polymerization under air.**

132 FRP and CP conducted under mild and low-cost conditions are the focus of this  
133 study. Five drops of the investigated formulation dripped into a round grinder with a  
134 thickness of 2 mm under air and one drop of the formulation deposited between two  
135 layers of polypropylene films in laminate (10 to 100 microns) were prepared for thick  
136 and thin samples respectively. Among them, the FRP of TMPTA and the CP of EPOX  
137 were carried out under LED@405 nm and under sunlight. Then, RT-FTIR (JASCO  
138 FTIR-4700) was adopted to monitor the polymerization of TMPTA ( $\sim 6150 \text{ cm}^{-1}$  in thick  
139 sample and  $\sim 1650 \text{ cm}^{-1}$  in thin sample) and EPOX ( $\sim 3770 \text{ cm}^{-1}$  in thick samples and  
140  $\sim 791 \text{ cm}^{-1}$  in thin samples) in real time. The specific preparation of the formulation is  
141 as follows: the two-component system (dye/EDB and dye/Iod) and the three-component  
142 system (dye/EDB/Iod) were fully mixed and dispersed into the monomers, and then  
143 stirred in the dark for 12 hours. And the effect of different dye contents on the  
144 photopolymerization efficiency was investigated. For the FRP of TMPTA with two-

145 component photoinitiating systems, the formulations were dye/EDB or dye/Iod 1%/1%,  
146 0.5%/1%, and 0.5%/0.5%, w/w. For the FRP of TMPTA with three-component systems,  
147 the formulations were dye/EDB/Iod 1%/1%/1%, 0.5%/1%/1%, 0.1%/1%/1%,  
148 0.05%/1%/1%, 0.5%/0.5%/0.5%, and 0.05%/0.5%/0.5%, w/w/w. For the CP of EPOX  
149 with three-component systems, the formulation was dye/EDB/Iod 0.1%1%/1% w/w/w.  
150 The final functional acrylate conversions (FCs) were obtained by the following  
151 equation:

$$152 \text{ Conversion (\%)} = \left(1 - \frac{A_t}{A_0}\right) \times 100\% \quad (6)$$

153 where  $A_0$  and  $A_t$  are the initial peak area before irradiation and the peak area after  
154 irradiation for  $t$  seconds, respectively.

155 In addition, the polymerization of TMPTA with the three-component  
156 Dye/EDB/Iod system under sunlight was also studied. The sunlight-induced  
157 polymerization experiments were carried out on December 15, 2023, from 10 am to 2  
158 pm, aligning with French time. The experiment site was in Mulhouse (+77 43 ' E, 47  
159 75 ' N), France, where the weather conditions were cloudy and the temperature varied  
160 between 1°C-8°C.

161

## 162 **2.5 ESR-ST experiments.**

163 To detect the radicals formed by reaction between dye and co-initiators (EDB or  
164 Iod), ESR-ST were carried out using an X-band spectrometer (Brook EMX-plus).  
165 Precisely, the solutions were prepared with the dye/EDB and dye/Iod systems with  
166 concentrations of  $2 \times 10^{-4}$  M, and the spin trap agent phenyl-*N-tert*-butylnitron (PBN)  
167 was added to them, and the concentration of PBN was about  $5 \times 10^{-4}$  M. Then, upon  
168 irradiation at 405 nm and under nitrogen, the generation of free radicals could be  
169 observed.

170

## 171 **2.6 Application of 3D printing.**

172 The 3D printing experiments were carried out using DLW. The photosensitive  
173 formulations containing dye-B1 and B6 were dripped into a self-made square tank, and  
174 irradiated by a computer-controlled laser diode 405 nm. The spot size was about 50

175 microns. The 3D pattern was observed and analyzed by a digital microscope.

176

## 177 **2.7 Computational procedure.**

178 Gaussian 03 was used to optimize the geometry and calculate the frontier  
179 molecular orbitals at the B3LYP/6-31G\* level, but also used to determine the triplet  
180 energy levels <sup>29</sup>.

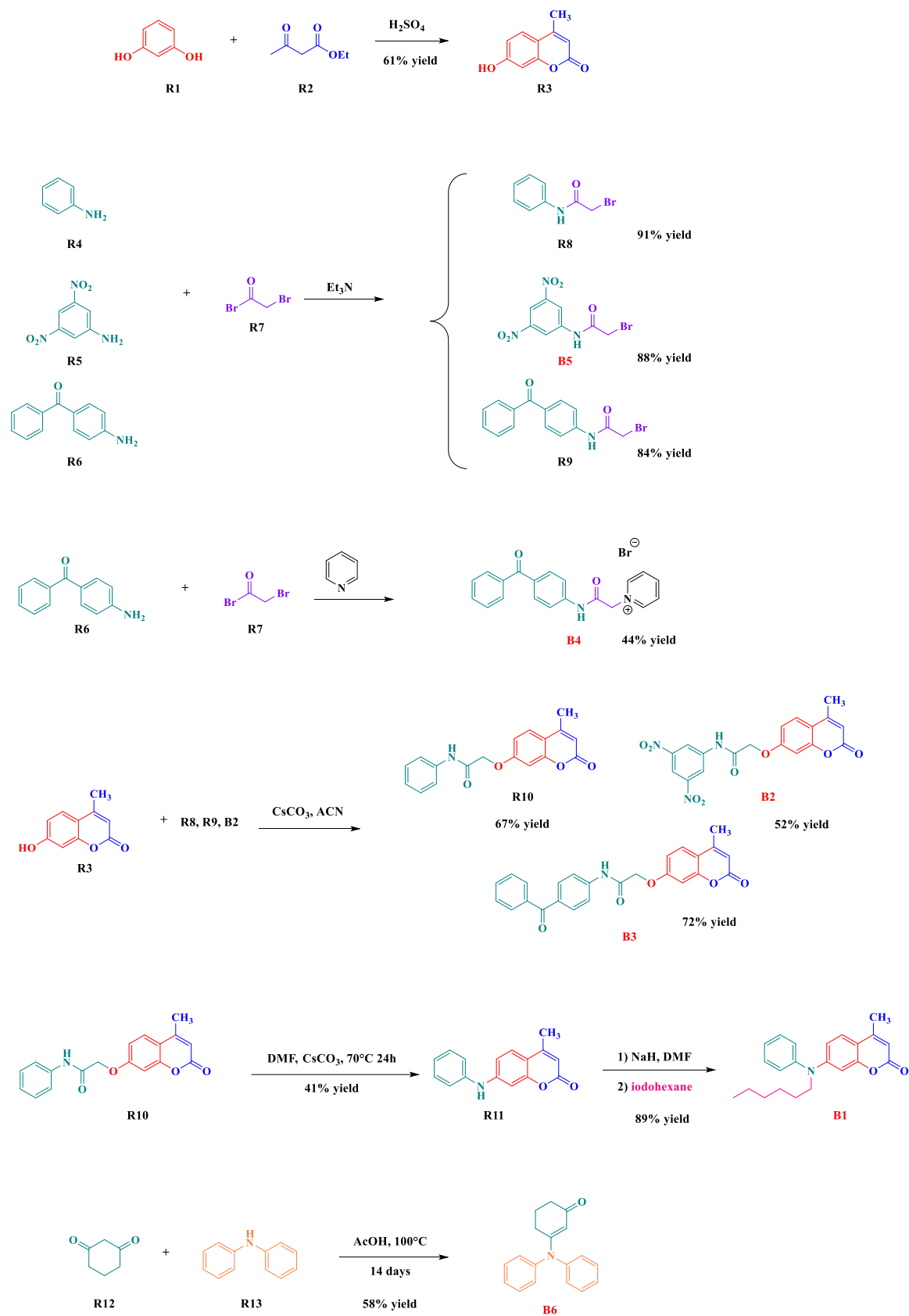
181

## 182 **3. Results and Discussion**

### 183 **3.1 Synthesis of the dyes.**

184 The various dyes investigated in this work were synthesized through a multistep  
185 synthesis approach. Notably, 7-hydroxy-4-methyl-2*H*-chromen-2-one R3 was prepared  
186 under acidic conditions, by mean of a Pechmann condensation between resorcinol R1  
187 and a  $\beta$ -ketoester (i.e. ethyl acetoacetate R2 in our case) in sulfuric acid <sup>30,31</sup>. The  
188 coumarin could be isolated in 61% yield. Parallel to this, R8, B5 and R9 were prepared  
189 starting from R4-R6, by condensation of the different aniline with bromoacetyl bromide  
190 R7 in the presence of triethylamine as the base. R8, B5 and R9 were respectively  
191 obtained with reaction yields of 91, 88 and 84%. In the case of 4-aminobenzophenone  
192 R6, by replacing triethylamine by pyridine as the base, a different product was obtained,  
193 resulting from the formation of the pyridinium salt, subsequently to the alkylation of  
194 the aniline moiety. B4 could be isolated in pure form in 44% yield. Finally, R10, B2  
195 and B3 were prepared by alkylation of R3 with R8, R9 and B2, enabling to prepare the  
196 substituted coumarins with reaction yields ranging between 52% for B2 up to B3 in 72%  
197 yield. The *N*-substituted 7-aminocoumarin R11 could be readily synthesized from R10  
198 by a tandem O  $\rightarrow$  N Smiles rearrangement-hydrolysis reaction using cesium carbonate  
199 as the base <sup>32</sup>. R11 was obtained in 41% yield (See Scheme 1). Finally, B1 was obtained  
200 by alkylation of the secondary amine of R11 with iodohexane, using sodium hydride as  
201 the base. B1 was isolated after purification in 89% yield. In the case of the *meta*-  
202 aminophenol B6, treatment of cyclohexane-1,3-dione R12 with diphenylamine R13 in  
203 acetic acid for 14 days enabled to prepare the *N,N*-diphenyl enaminone B6 in 58% yield.





204

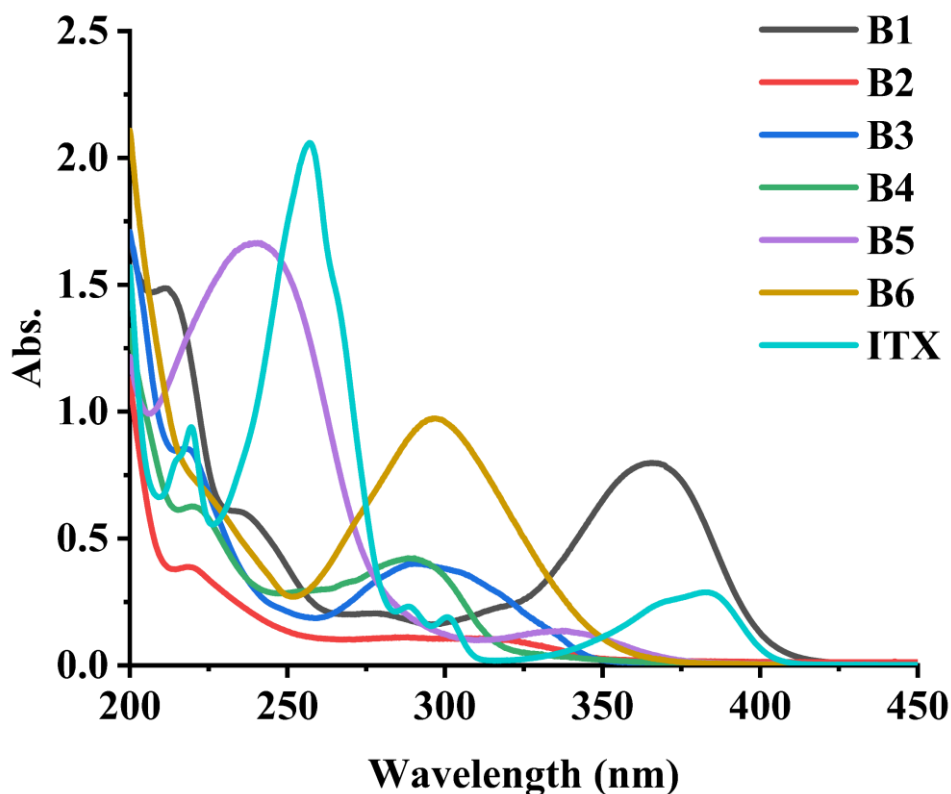
205

206

Scheme 1. Synthetic routes to B1-B6.

207 **3.2 Light absorption properties.**

208 The light absorption properties of the six dyes were determined in acetonitrile. The  
209 concentration of dyes was  $2.5 \times 10^{-5}$  M, and their UV-visible absorption spectra are  
210 shown in Figure 2. The maximum absorption wavelength ( $\lambda_{\max}$ ) and the maximum  
211 molar extinction coefficient ( $\epsilon_{\max}$ ) of the six dyes and the  $\epsilon_{405 \text{ nm}}$  at 405 nm are  
212 summarized in Table 1. Obviously, the  $\lambda_{\max}$  of the six dyes and ITX were between 300-  
213 400 nm, and dye-B1 and dye-B6 exhibited the largest  $\epsilon_{\max}$ , which were  $15940 \text{ M}^{-1}\text{cm}^{-1}$   
214 and  $19420 \text{ M}^{-1}\text{cm}^{-1}$ , respectively. These molar extinction coefficients were higher than  
215 the commercial photoinitiator ITX, and the  $\epsilon_{405\text{nm}}$  of dye-B1 was the largest in this series  
216 of dyes. This result is consistent with their high initiation performance in  
217 photopolymerization (LED@405 nm) as discussed below, so that dye-B1 was also  
218 selected as the appropriate photosensitizer for sunlight-induced polymerization. In  
219 addition, the  $\epsilon_{\max}$  and  $\epsilon_{405 \text{ nm}}$  of dye-B2, B3, B4, and B5 were low, and their  
220 photoinitiation abilities in photopolymerization were poor correspondingly as shown  
221 below.



222

223 **Figure 2.** UV-visible absorption spectra of dyes in acetonitrile (B1-B6 and ITX).

224

225

**Table 1.** Light absorption characteristics of dyes.

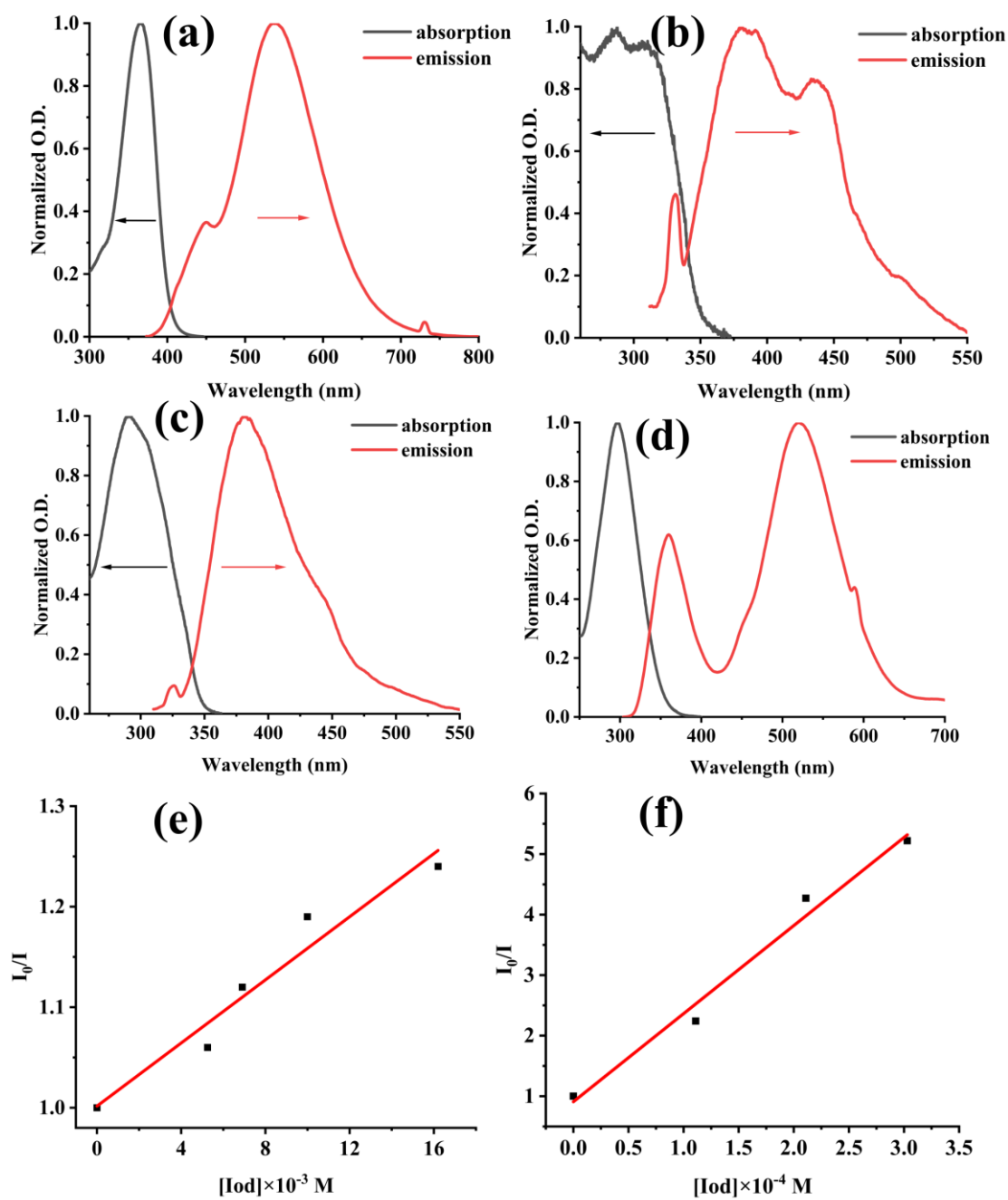
<b>PIs</b>	$\lambda_{\text{max}}$ (nm)	$\epsilon_{\text{max}}$ (M <sup>-1</sup> cm <sup>-1</sup> )	$\epsilon_{405}$ (M <sup>-1</sup> cm <sup>-1</sup> )
B1	370	15940	1450
B2	310	2080	270
B3	290	8000	80
B4	290	8410	70
B5	340	2690	90
B6	300	19420	60
ITX	390	5890	1000

226

227 **3.3 Fluorescence properties (i.e. fluorescence spectra, fluorescence excited state**  
 228 **lifetimes, fluorescence quenching experiments) and chemical mechanism in**  
 229 **electron transfer reactions.**

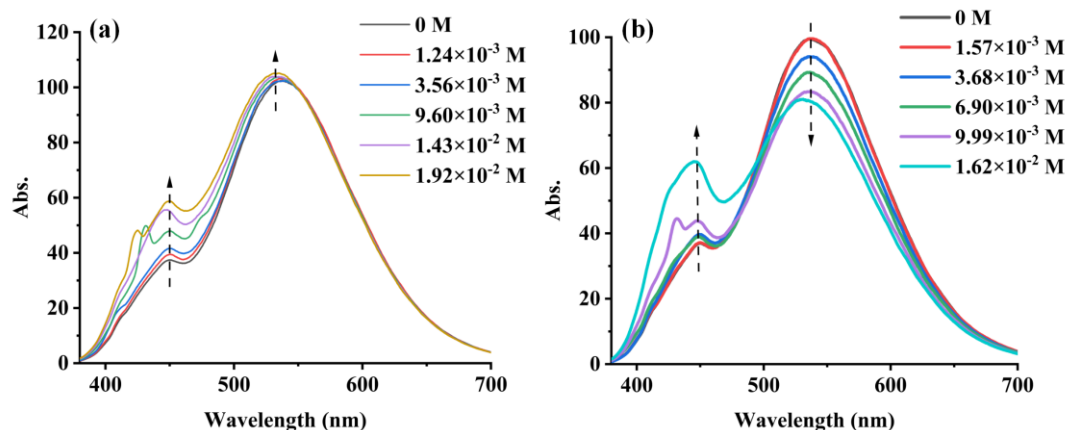
230 Parallel to the absorption properties, the fluorescence spectra of the six dyes in  
 231 acetonitrile were determined as shown in Figure S2. Dye-B5 demonstrated no or only  
 232 a weak fluorescence. On the contrary, dye-B1 and B6 exhibited a strong fluorescence  
 233 in the range of 400-700 nm and these two dyes showed a long fluorescence excited state  
 234 lifetime (See Figure S3), which may be an important reason for their good  
 235 photoinitiation abilities. The interaction between dyes and co-initiators and various  
 236 parameters in the electron transfer reaction are summarized in Table 2. Among them,  
 237 the  $E_{S1}$  was calculated by the intersection between the normalized fluorescence  
 238 spectrum and the UV-visible absorption spectrum of the dye (See Figure 3). The  $E_{\text{ox}}$   
 239 and  $E_{\text{red}}$  potentials of the six dyes were determined by CV (See Figure S4). From Figure  
 240 S4, the oxidation and reduction peaks of the six dyes studied can be clearly observed.  
 241 According to equations (2) and (3), the  $\Delta G^{S1}$  of electron transfer between dyes and  
 242 additives were calculated, and the values are listed in Table 2. From the values, the  $\Delta G^{S1}$   
 243 of all dyes were negative, indicating that the reactions of dye/EDB and dye/Iod are  
 244 feasible.

245 In addition, the interaction between dyes and EDB/Iod were further characterized  
246 by fluorescence quenching experiments. The fluorescence quenching spectra obtained  
247 with the dye/EDB and dye/Iod systems in acetonitrile are shown in Figures 4 and S5.  
248 Figure 4 shows the change of fluorescence emission caused by the interaction between  
249 dye-B1 and co-initiators. After the addition of a certain amount of EDB to the dye, the  
250 fluorescence intensity slightly increased (See Figure 4(a)). The possible reason was that  
251 dye-B1 reacted with EDB to generate a new fluorescent product, which increased the  
252 fluorescence intensity. However, after the addition of a certain amount of Iod to the dye,  
253 the intensity of dye fluorescence decreased obviously (See Figure 4(b)), which  
254 indicated that Iod had an efficient fluorescence quenching effect on dye-B1. Therefore,  
255 the  $K_{sv}$  of dye/Iod could be determined by fluorescence quenching (See Figures 3 and  
256 S6). Similarly, dye-B2, B3 and B6 all showed a downward trend in strength after the  
257 addition of co-initiators (See Figure S5), and the corresponding  $K_{sv}$  are summarized in  
258 Table 2.  
259



260

261 **Figure 3.** (a)  $E_{S1}$  determination in acetonitrile for: (a) dye-B1; (b) dye-B2; (c) dye-B3  
 262 and (d) dye-B6 respectively. Stern – Volmer treatment for fluorescence quenching of  
 263 (e) dye-B1/Iod and (f) dye-B2/Iod.



264

265 **Figure 4.** Fluorescence quenching of (a) dye-B1 and EDB, (b) dye-B1 and Iod in  
 266 acetonitrile.

267

268 **Table 2.** Parameters of the chemical mechanisms associated with dyes in acetonitrile.

	Dye-B1	Dye-B2	Dye-B3	Dye-B4	Dye-B5	Dye-B6
$E_{LUMO}$ (eV) <sup>a</sup>	-1.24	-3.13	-1.77	-6.21	-3.05	-0.89
$E_{HOMO}$ (eV) <sup>a</sup>	-5.57	-6.69	-6.61	-8.87	-7.76	-5.69
$E_{ox}$ (eV)	1.19	0.96	0.93	0.93	1.00	1.32
$E_{red}$ (eV)	-	-0.95	-0.74	-1.39	-1.03	-1.36
$E_{S1}$ (eV)	3.07	3.64	3.65	3.95	-	3.69
$\Delta G^{S1}_{EDB}$	-	-1.69	-1.91	-1.56	-	-1.60
$\Delta G^{S1}_{Iod}$	-1.18	-1.98	-2.02	-2.32	-	-1.67
$E_{T1}$ (eV) <sup>b</sup>	2.41	2.56	2.65	2.48	2.33	2.41
$\Delta G^{T1}_{EDB}$	-	-0.61	-0.91	-0.09	-0.30	-0.06
$\Delta G^{T1}_{Iod}$	-1.92	-2.30	-2.42	-2.25	-2.03	-1.80
$K_{sv}$ (EDB)	-	618.94	-	-	-	1039.21
$K_{sv}$ (Iod)	15.70	145.55	22.39	-	-	18.29
$\phi_{et}$ (EDB)	-	0.98	-	-	-	0.99
$\phi_{et}$ (Iod)	0.39	0.85	0.47	-	-	0.42

269

a: HOMO and LUMO energies are computed at a MPW1PW91/6-31G\* level of theory on

270

structures optimized at a UB3LYP/6-31G\* level of theory.

271

b: Triplet energies are computed at a UB3LYP/6-31G\* level of theory.

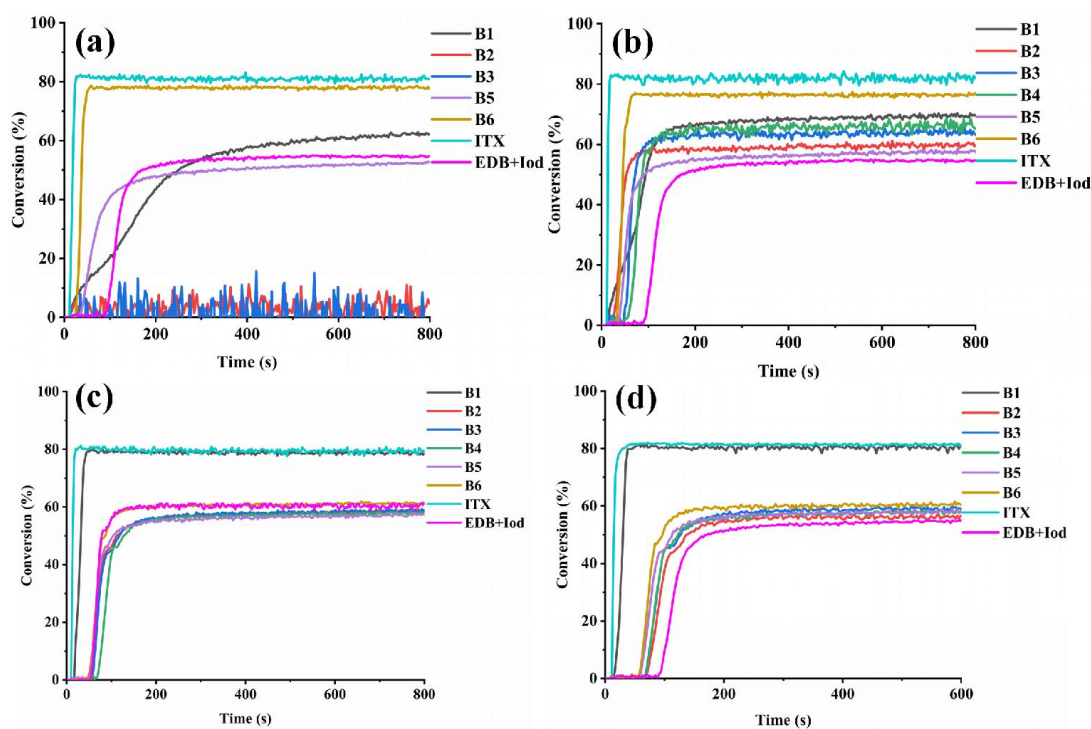
272

### 273 **3.4 FRP kinetics under near UV/visible-light irradiation in TMPTA.**

274 To investigate the photoinitiation abilities of the six dyes in photopolymerization,  
275 the photopolymerization profiles of two and three-component systems were determined  
276 upon irradiation at 405 nm with a LED, and the conversions of acrylate double bond  
277 functional groups were monitored using RT-FTIR at room temperature. The results  
278 showed that the FCs obtained with the three-component systems were higher than that  
279 obtained with the two-component systems (See Table S1 and Figure S7 for the  
280 conversions of thick samples (2 mm) which could be deeply cured (See Figure S9), and  
281 Table S2 and Figure S8 for the conversions of thin samples (10 to 100 microns)). It was  
282 particularly noted that the dye-free two-component system EDB/Iod (1%/1% w/w) was  
283 used as a reference system. In fact, dyes could only initiate a polymerization of  
284 monomers in combination with co-initiators such as EDB or Iod. The specific chemical  
285 mechanism is given in section 3.10. Considering that the three-component  
286 photoinitiating systems showed the higher photoinitiation abilities than their two-  
287 component analogues, the amounts of co-initiators EDB/Iod (1%/1% w/w) were fixed  
288 to 1wt% by the control variable method in this study, and the influence of different  
289 contents (relative to monomer) of dyes on photopolymerization of the three-component  
290 system was studied. As shown in Figures 5 (a-d), the photopolymerization profiles of  
291 thick samples with different contents of dyes (1wt%, 0.5wt%, 0.1wt%, and 0.05wt%)  
292 were different, and the FCs of acrylate functional groups are summarized in Table 3.

293 For dye-B1, by decreasing the dye content, the formulations became clearer and  
294 more transparent, and the conversions increased from ~60% to 80%, which finally  
295 showed an upward trend. When the dye contents were set to 0.1% and 0.05%, the  
296 conversions were almost similar to that obtained with the commercial initiator ITX  
297 (~80%), which was much higher than 55% for the reference EDB/Iod (1%/1% w/w)  
298 system in blank control group. This is undoubtedly the most effective photoinitiators  
299 among the series of dyes investigated in this work. For dye-B6, the monomer  
300 conversions decreased with the reduction of the dye contents. When the concentration  
301 was set to 1%, the highest conversion reached 79%. For dyes-B2, B3, and B4, when the

302 content was set to 1wt%, they cannot be completely dissolved in the monomer, which  
 303 led to a poor light penetration, thus the monomer conversion was extremely low. When  
 304 the contents were set to 0.5wt%, 0.1wt%, and 0.05wt%, the conversions basically  
 305 maintained between 56% and 68%, which were lower than that of ITX, but slightly  
 306 higher than that of blank control group EDB/Iod (1%/1% w/w) by 55%. The  
 307 conversions of dye-B5 in all content gradients were between 50 and 60%, which were  
 308 close to that obtained with the dye-B2, B3, and B4. Due to the fact that the conversions  
 309 obtained with these four dyes were lower than that obtained with dye-B1 and B6, these  
 310 four dyes were excluded from the follow-up research.



311

312 **Figure 5.** FRP profiles of TMPTA for thick sample (about 2 mm) under LED@405 nm  
 313 irradiation. Initiated by (a) dye/EDB/Iod 1%/1%/1% w/w/w; (b) dye/EDB/Iod  
 314 0.5%/1%/1% w/w/w; (c) dye/EDB/Iod 0.1%/1%/1% w/w/w; and (d) dye/EDB/Iod  
 315 0.05%/1%/1% w/w/w.

316

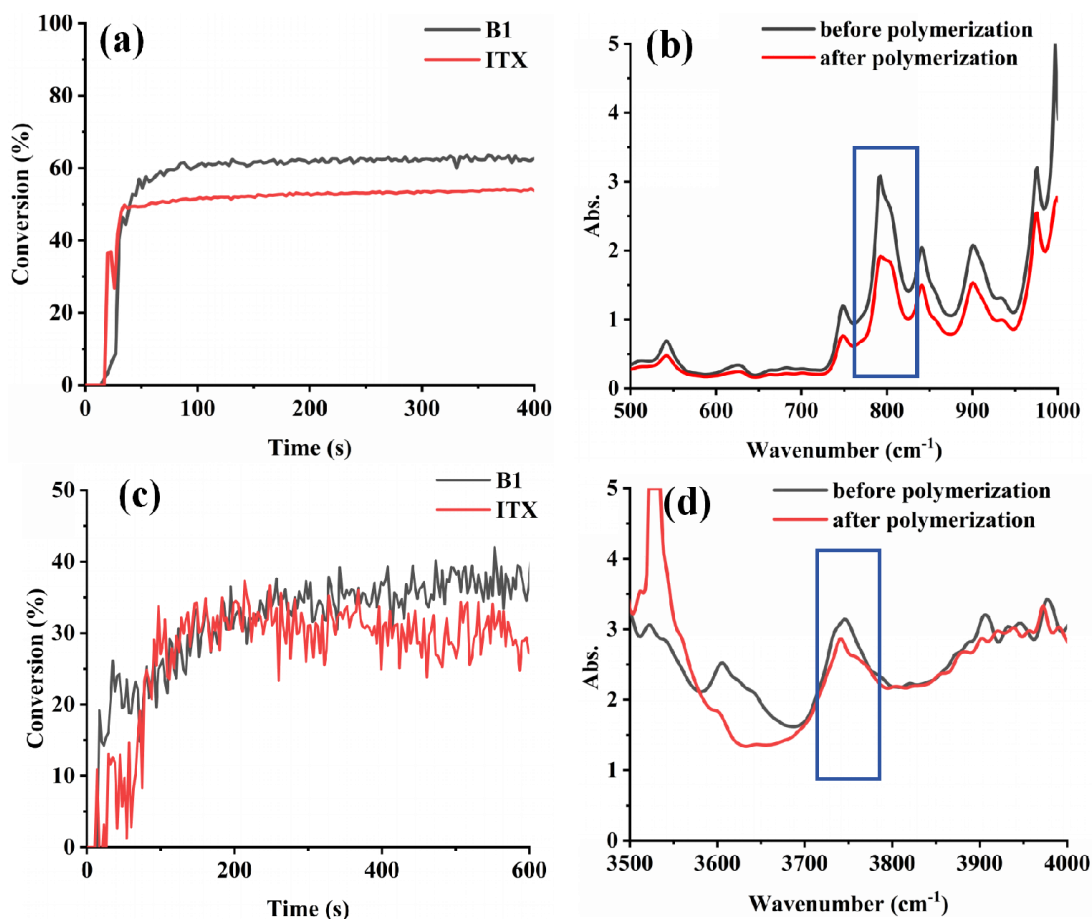
### 317 **3.5 Metal-free cationic free radical polymerization of EPOX.**

318 The photoinitiation ability of the three-component system based on dye-B1 in



319 EPOX was examined at 405 nm and the results are shown in Figures 6 (a-d). The  
320 conversions obtained with the different dyes and ITX are summarized in Table 4. The  
321 Dye-B1/EDB/Iod 0.1%/1%/1% w/w/w (relative to monomer EPOX) three-component  
322 system showed a higher photoinitiation ability than the commercial initiator ITX in  
323 both thin and thick samples. It is worth mentioning that a high monomer conversion  
324 rate could be still achieved when the dye content was only 0.1wt%. Among them, the  
325 monomer conversion for thin samples (See Figure 6 (a)) was more than 60% after 100  
326 seconds of irradiation, and the maximum monomer conversion in thick samples (See  
327 Figure 6 (c)) was close to 40% after 600 seconds. In addition, under the same conditions,  
328 the blank control EDB/Iod (1%/1% w/w) could not initiate the polymerization of EPOX,  
329 indicating that dye-B1 played a crucial role in the cationic photopolymerization (all  
330 operations were carried out at room temperature). The possible reason is that dye-B1  
331 reacts with EDB and Iod to produce radical cations ( $\text{dye}^{\bullet+}$ ). The chemical mechanism  
332 is shown in Section 3.10.

333

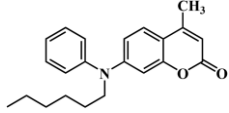
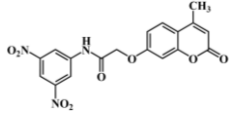
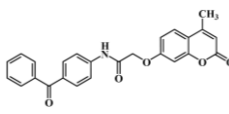
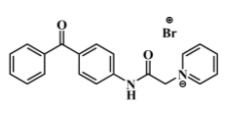
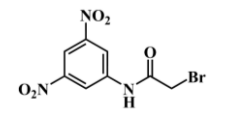
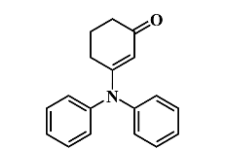
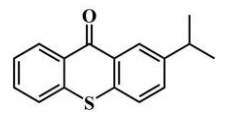


334

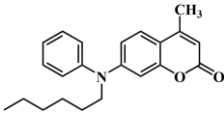
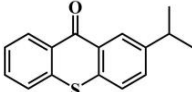
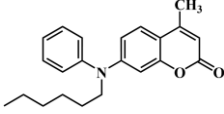
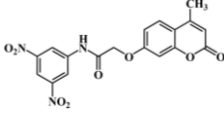
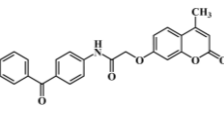
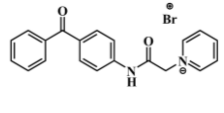
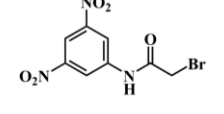
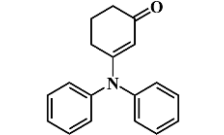
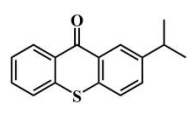
335 **Figure 6.** CP profiles of EPOX upon exposure to LED@405 nm irradiation in dye-  
 336 B1/EDB/Iod 0.1/1/1 w/w/w. (a) for thin sample (10 to 100 microns) in laminate; (b) In  
 337 RT-FTIR absorbance spectrum for EPOX for thin sample (10 to 100 microns) in  
 338 laminate to irradiation for 100 seconds; (c) for thick sample (about 2 mm); (d) In RT-  
 339 FTIR absorbance spectra for EPOX for thick sample (about 2 mm) to irradiation for  
 340 100 seconds. The irradiation starts at t = 10 seconds.

341

342 **Table 3.** Summary of the thick sample FCs at LED@405 nm for TMPTA using three-  
 343 component systems: dye/EDB/Iod.

No.	Structure of dyes	Dye(1%)+EDB	Dye(0.5%)+EDB	Dye(0.1%)+EDB	Dye(0.05%)+EDB
		(1%)+Iod(1%)	(1%)+Iod(1%)	(1%)+Iod(1%)	(1%)+Iod(1%)
FCs (%)					
B1		62	60	80	80
B2		0	60	58	56
B3		0	64	58	58
B4		-	68	57	58
B5		53	58	57	58
B6		79	77	62	61
ITX		81	81	80	80
EDB		55	55	55	55
+Iod					

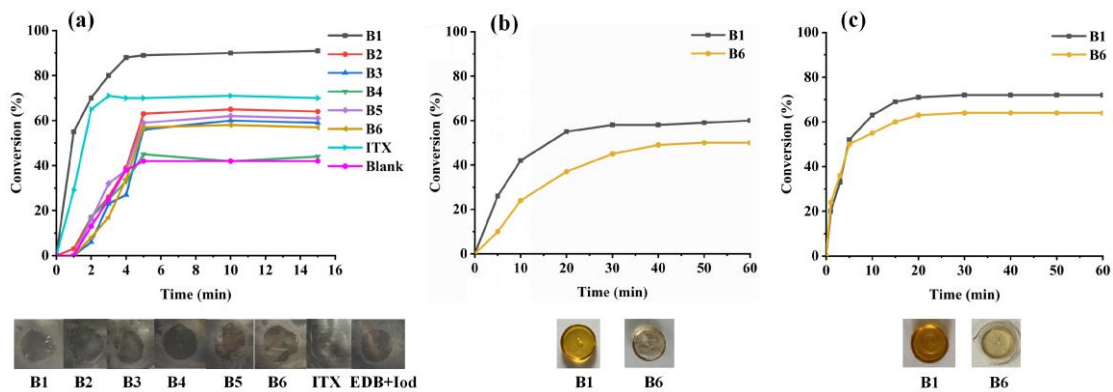
344 **Table 4.** Summary of the FCs under LED@405 nm for metal-free CP of EPOX and  
 345 sunlight-induced polymerization for TMPTA using three-component systems: dye  
 346 /EDB/Iod.

<b>Metal-free cationic free radical polymerization of EPOX (The formulation is Dye(0.1%)+EDB(1%)+Iod(1%))</b>				
No.	Structure of dyes	FCs (%) of thin sample	FCs (%) of thick sample	
B1		63	40	
ITX		54	30	
<b>High performance sunlight-induced polymerization of TMPTA (The formulation is Dye(0.1%)+EDB(2%)+Iod(2%))</b>				
No.	Structure of dyes	FCs (%) of thin sample in laminate	FCs (%) of thick sample in the air	FCs (%) of thick sample in laminate
B1		90	60	71
B2		65		
B3		60		
B4		45		
B5		61		
B6		57	50	64
ITX		71		

347

**348 3.6 High-performance sunlight-induced polymerization under air in three-**  
**349 component systems of TMPTA.**

350 Based on the high-performance of the six dyes upon excitation at 405 nm, the  
351 experiment of sunlight-induced polymerization was tested on December 15, 2023 at 10  
352 am - 2 pm in Mulhouse, France. The specific experimental conditions were as follows:  
353 for the thin samples (10 to 100 microns), the three-component system Dye/EDB/Iod  
354 0.1%/2%/2% w/w/w was used for photopolymerization under sunlight, and the  
355 monomer was TMPTA. As shown in Figure 7(a), the conversions of all samples reached  
356 the maximum within 5 minutes, especially the conversion of dye-B1 was as high as 90%  
357 within 5 minutes, which was much higher than that obtained with the commercial  
358 initiator ITX (71%) and the blank (EDB/Iod 2%/2%, w/w) group (42%). For thick  
359 samples, as shown in Figure 7(b), the maximum conversions of samples containing  
360 dye-B1 and dye-B6 were 60% and 50% respectively within 60 minutes when the 2 mm  
361 thick resin sample in open mold (no protection against oxygen inhibition) were exposed  
362 to outdoor sunlight. More interestingly, when the open mold of the thick sample was  
363 closed and isolated from oxygen, it was found that the polymerization rate of dye-B1  
364 and B6 were obviously accelerated under sunlight, and the FCs were also improved,  
365 the maximum conversions were 71% and 64% for the samples containing dye-B1 and  
366 dye-B6 within 60 minutes (See Figure 7(c)). The conversions of all samples under  
367 sunlight are summarized in Table 4. Markedly, for the polymerized samples shown at  
368 the bottom of Figure 7, it can be seen that the photocuring was complete, which proved  
369 that the six dyes examined in this study showed an excellent photoinitiation ability  
370 under sunlight and thus under mild irradiation conditions and can be used as efficient  
371 photoinitiators.



372

373 **Figure 7.** Sunlight polymerization profiles of TMPTA for (a) thin sample (10 to 100  
 374 microns) in laminate, (b) thick sample (2 mm) under sunlight in the air and (c) thick  
 375 sample (2 mm) under sunlight in laminate. Initiated by dye/EDB/Iod 0.1%/2%/2%  
 376 w/w/w.

377

### 378 **3.7 Steady state photolysis experiments of dye alone, dye/EDB and dye/Iod** 379 **photoinitiation systems.**

380 To reveal the interactions existing between the dyes and EDB/Iod more  
 381 comprehensively and the stability of individual dyes, photolysis experiments were  
 382 carried out for the dye-alone, dye/EDB, and dye/Iod in acetonitrile under LED@405  
 383 nm. The results are shown in Figures S10, S11, and S12. It's worth noting that the  
 384 concentration of dye was set to  $2.5 \times 10^{-5}$  M, and the concentrations of EDB and Iod  
 385 were set to  $5 \times 10^{-5}$  M. From Figure S10, after irradiation for 25 minutes, the intensity  
 386 of the UV spectra of all dyes in the absence of co-initiator (dye-alone) basically not  
 387 decreased, indicating that a dye alone demonstrated a good light stability. Remarkably,  
 388 for the dye/EDB system after a long time of irradiation, the photolysis was not obvious  
 389 (Figure S11), indicating that the photochemical interaction between dye and EDB was  
 390 very slow. In the dye/Iod system, only dye-B1 showed an obvious dramatic decrease in  
 391 the absorption spectra after being irradiated by LED@405 nm for 25 minutes (Figure  
 392 S12(a)). Therefore, dye-B1 can be considered as the most effective dye among all the  
 393 six dyes, which was verified during the photopolymerization with TMPTA and EPOX.

394

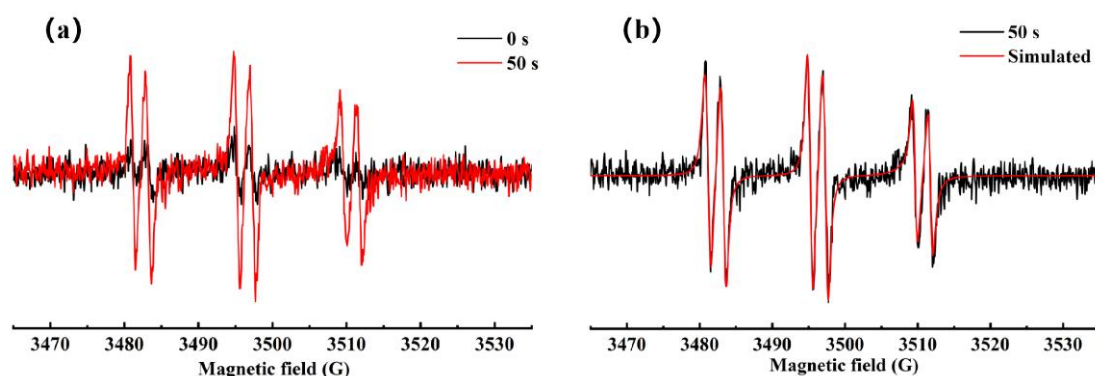
### 395 **3.8 Sunlight stability experiments.**

396 The stability of photoinitiators is essential for practical application. To verify the  
397 stability of the six dyes under sunlight, their stabilities were tested upon exposure to  
398 sunlight for 120 minutes. As shown in Figure S13, all dyes demonstrated an excellent  
399 stability in acetonitrile, and after a long period of steady-state photolysis, the UV-visible  
400 absorption spectra hardly changed. It thus revealed that the different dye exhibit a good  
401 stability under sunlight, which is the basis for long-term storage, transportation, and use  
402 under sunlight.

403

### 404 3.9 ESR-ST experiments.

405 To study the free radicals produced by interaction between dyes and additives  
406 during photopolymerization, ESR-ST experiments were carried out at room  
407 temperature under LED@405 nm. As shown in Figure 8, PBN successfully captured  
408 the radical (100%) of dye-B6/Iod in *tert*-butylbenzene solution (under nitrogen  
409 atmosphere), and its hyperfine coupling constants were  $\alpha_N = 14.3$  G and  $\alpha_H = 2.1$  G  
410 (accuracy  $\pm 0.1$  G), which may be assigned to phenyl radicals<sup>33</sup>. Especially, ESR-ST  
411 experiments done on the dye-B6/EDB system revealed no obvious signals (See Figure  
412 S14), consistent with the steady-state photolysis experiments done under the irradiation  
413 of LED@405 nm (See Figure S11(f)) and the low photopolymerization conversion.



414

415 **Figure 8.** ESR-ST spectra of the radical adducts (in *tert*-butylbenzene under nitrogen  
416 atmosphere), (a) and (b) dye-B6/Iod.

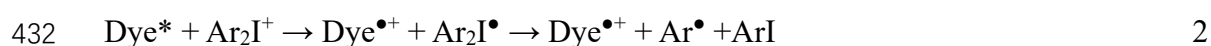
417

### 418 3.10 Photoinitiation mechanisms and theoretical calculations of dyes.

419 According to our previous study, the chemical mechanism of photopolymerization

420 was determined and summarized as the following five reactions. The chemical  
 421 mechanism was mainly the results of a redox reaction between the dyes and EDB and  
 422 Iod in the excited state. First of all, the dye in the ground state was promoted in the  
 423 excited state (dye\*) after light irradiation (See reaction 1), and then the excited dye  
 424 reacted with EDB and Iod (See reactions 2 and 3). Interestingly, dye<sup>•+</sup> produced in  
 425 reaction 2 and Dye-H<sup>•</sup> produced in reaction 3 can be oxidized and reduced by EDB and  
 426 Iod to the ground state dye for regeneration, thus completing the catalytic cycle (See  
 427 reactions 4 and 5). In the whole reaction process, free radical polymerization was  
 428 initiated by free radicals, while cationic polymerization was initiated by cations  
 429 generated in the reaction process.

430



436

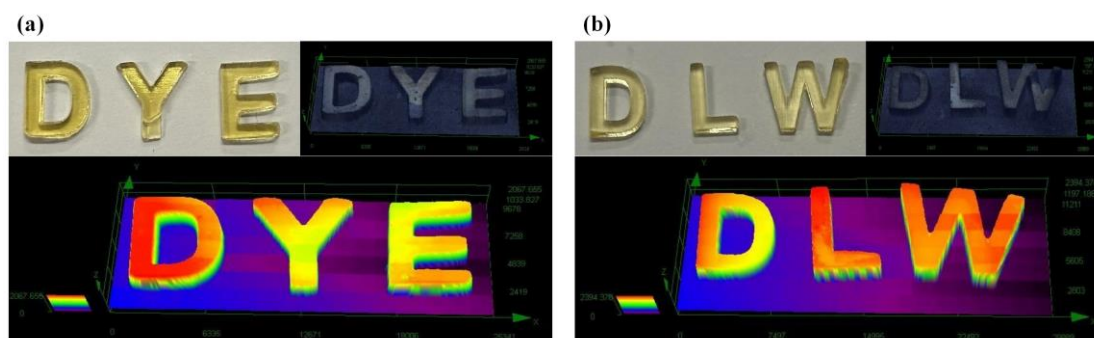
437 It's worth noting that in the case of the three-component system based on the  
 438 different dyes, the initiation behavior in FRP and CP processes may be different, and  
 439 the oxidation and reduction cycles experienced by dyes can be discussed thanks to the  
 440 results obtained by theoretical calculations concerning the contour plots of the frontier  
 441 molecular orbital but also thanks to the different photochemical parameters. One  
 442 important theoretical parameter was  $E_{S1}$ , and the second one was  $E_{T1}$ . Indeed, long-  
 443 living triplet excited states favor the generation of free radicals by providing more time  
 444 for the dye to react with the additives so that the polymerization process can be more  
 445 effectively promoted<sup>13</sup>.  $E_{T1}$  were obtained at a UB3LYP/6-31G\* level of theory.  
 446 HOMO and LUMO energies were obtained at a MPW1PW91/6-31G\* level of theory  
 447 (See Table 2). It can be concluded that the excellent photoinitiation ability of dye-B1  
 448 can be attributed to its high molar extinction coefficient, the high energies of its HOMO  
 449 and LUMO energy levels, and even its excellent photochemical reactivity in the excited

450 state.  $E_{T1}$  of dye-B5 was the lowest, which was in agreement well with its poor  
451 photoinitiation ability. However, dyes-B2, B3, and B4 with high  $E_{T1}$  did not show  
452 satisfactory photoinitiation ability, which may be due to their low molar extinction  
453 coefficients.

454

### 455 **3.11 Application in 3D printing.**

456 Dye-B1 and dye-B6 were selected as appropriate candidates for practical  
457 applications, and the formulations (Dye-B1/EDB/Iod 0.1w%/1w%/1w% and Dye-  
458 B6/EDB/Iod 1w%/1w%/1w%) were formed with co-initiators and irradiated with a  
459 laser diode at 405 nm. The whole process was carried out at room temperature.  
460 Interestingly, 3D patterns with a high precision and a clear outline (Dye-B1 to "DYE"  
461 is shown in Figure 9 (a) and dye-B6 to "DLW" is shown in Figure 9 (b)) were obtained  
462 (the printed sizes are 7 mm in length, 5 mm in width and 2 mm in height), and its surface  
463 was observed by numerical optical microscopy, and a 3D pattern with a smooth surface  
464 and an excellent spatial resolution was successfully manufactured in a short time. The  
465 success of the 3D printing experiments, the possibility to promote sunlight-induced  
466 polymerization with these dyes make these structures promising candidates for future  
467 applications.



468

469 **Figure 9.** Digital photos of 3D printing objects. (a) dye-B1/EDB/Iod; (b) dye-  
470 B6/EDB/Iod; TMPTA as monomer.

471

## 472 **4. Conclusion**

473 In summary, six new metal-free dyes were designed and synthesized, and  
474 successfully combined with EDB and Iod to form three-component photoinitiating



475 systems. Notably, under LED@405 nm irradiation, these photoinitiating systems  
476 successfully generated active free radicals, initiating the FRP of TMPTA and the CP of  
477 EPOX. Particularly noteworthy was their photoinitiation abilities, enabling the  
478 initiation of the FRP of TMPTA under sunlight, with dye-B1 achieving an  
479 unprecedented 90% monomer conversion within 5 minutes. Furthermore, all dyes  
480 exhibited a remarkable light stability under sunlight, a crucial attribute for practical  
481 applications. The photoinitiation properties of the dyes were comprehensively validated  
482 through both theoretical and experimental approaches, including steady-state  
483 photolysis, excited-state fluorescence quenching tests, and theoretical calculations.  
484 Lastly, the dye-B1/EDB/Iod and dye-B6/EDB/Iod three-component systems were  
485 successfully applied to 3D printing. This work not only showcases the potential of the  
486 metal-free dyes to initiate polymerization under sunlight, but also addresses limitations  
487 associated with visible light LEDs and the traditional UV light sources in  
488 photopolymerization and photocuring. By saving energy and aligning with the  
489 principles of sustainable development in green chemistry, sunlight-induced  
490 polymerization holds tremendous promise for diverse applications in photocuring.

491

492

493

#### 494 **Conflicts of interest**

495 The authors declare no competing financial interest.

#### 496 **Acknowledgements**

497 This research project is supported by China Scholarship Council (CSC)  
498 (No.202208220049).

499

500

501

502

503

504

505

506 **References**

- 507 1. Corrigan, N., *et al.*, *Chem Soc Rev* (2016) **45** (22), 6165
- 508 2. Giacomo Ciamician *Science* (1912) **26**, 385
- 509 3. Guo, X., *et al.*, *Angew Chem Int Ed Engl* (2023) **62** (27), e202301242
- 510 4. Paula Militello, M., *et al.*, *Solar Energy* (2023) **258**, 270
- 511 5. Xie, H., *et al.*, *Progress in Polymer Science* (2019) **95**, 32
- 512 6. Li, T., *et al.*, *Journal of Solid State Electrochemistry* (2013) **17** (10), 2651
- 513 7. Li, L., *et al.*, *Journal of Electronic Materials* (2014) **43** (7), 2588
- 514 8. Sun, K., *et al.*, *Journal of Photochemistry and Photobiology C: Photochemistry*
- 515 *Reviews* (2023) **57**
- 516 9. Chen, J., *et al.*, *Polymer Chemistry* (2023) **14** (4), 486
- 517 10. Xu, J., *et al.*, *J Am Chem Soc* (2014) **136** (14), 5508
- 518 11. Huang, Y., *et al.*, *ACS Macro Letters* (2018) **7** (2), 184
- 519 12. Jordan C. Theriot, *et al.*, *Science* (2016) **352**, 1082
- 520 13. Jiang, J., *et al.*, *Angew Chem Int Ed Engl* (2018) **57** (37), 12037
- 521 14. Eklund, A. G., *et al.*, *J Air Waste Manag Assoc* (2013) **63** (11), 1235
- 522 15. MacKie, R. M., *Prog Biophys Mol Biol* (2006) **92** (1), 92
- 523 16. Bella, F., *et al.*, *The Journal of Physical Chemistry C* (2013) **117** (40), 20421
- 524 17. Yu, J., *et al.*, *Macromolecules* (2019) **52** (4), 1707
- 525 18. Allegranza, M. L., *et al.*, *Polymer Chemistry* (2016) **7** (43), 6626
- 526 19. Ma, C., *et al.*, *Adv Sci (Weinh)* (2019) **6** (13), 1900085
- 527 20. Fang, W. W., *et al.*, *Nat Commun* (2023) **14** (1), 2891
- 528 21. Fouassier, J. P., *et al.*, *Progress in Organic Coatings* (2003) **47** (1), 16
- 529 22. Schmitt, M., *Nanoscale* (2015) **7** (21), 9532
- 530 23. Li, J., *et al.*, *Progress in Organic Coatings* (2022) **171**
- 531 24. Zhang, Y., *et al.*, *Chem Soc Rev* (2021) **50** (6), 3824
- 532 25. Xiao, P., *et al.*, *Progress in Polymer Science* (2015) **41**, 32
- 533 26. Pei, H.-W., *et al.*, *Polymer Chemistry* (2024)

534 27. Dieter Rehm, A. W., *ISRAEL JOURNAL OF CHEMISTRY* (1970) **8**, 259

535 28. Ley, C., *et al.*, *Polymer* (2023) **268**

536 29. Frisch, M. J., *et al.*, (2003)

537 30. Mitth, *Berichte Der Deutschen Chemischen Gesellschaft* (1884), 929

538 31. Zambare, A. S., *et al.*, *Current Organic Chemistry* (2016) **20** (19)

539 32. Lippe, D. S., *et al.*, *ACS omega* (2022) **7** (39), 35269

540 33. Versace, D.-L., *et al.*, *Macromolecules* (2013) **46** (22), 8808

541

542 **TOC graphic:**

